Available online at www.sciencedirect.com
ScienceDirect
Ceramics International 37 (2011) 3547–3556
CERAMICS INTERNATIONAL
www.elsevier.com/locate/ceramint

Role of immiscible and miscible second phases on the sintering kinetics and microstructural development of nano-crystalline α-Al_2O_3-based materials

Paola Palmero [a,*], Frank Kern [b], Mariangela Lombardi [a,1], Rainer Gadow [b]

[a] Dept. Materials Science and Chemical Engineering, INSTM – R.U. PoliTO – LINCE Lab., Politecnico di Torino, Corso Duca degli Abruzzi, 24, 10129 Torino, Italy
[b] University of Stuttgart, IFKB, Allmandring 7b, D-70569 Stuttgart, Germany

Received 27 May 2011; accepted 6 June 2011
Available online 13 June 2011

Abstract

An ultra-fine alumina powder was doped with yttrium or zirconium chloride to produce Al_2O_3–5 vol.%ZrO_2 (AZ-5) and Al_2O_3–5 vol.%YAG (AY-5) composite powders. Composite samples and pure alumina, used as a reference, were submitted to dilatometric analyses up to 1500–1550 °C at 2, 5 and 10 °C/min for supplying the data required for the modeling of their sintering behaviour. The best fit for the three samples was obtained by applying an Avrami–Erofeev nucleation and growth model (An) and a subsequent power law reaction (AnFn). The evolution of the activation energy with densification is given for the three samples, as well as the prediction of their best sintering conditions. Finally, densification mechanism for the immiscible (AZ-5) and miscible (AY-5) systems are hypothesized and correlated with their final microstructures.

Keywords: A. Grain growth; B. Microstructure-final; B. Nanocomposites; Al_2O_3–ZrO_2; Al_2O_3–YAG; Sintering kinetics

1. Introduction

In the last years, alumina-based nanocomposites have been widely investigated, since they show enhanced mechanical properties at room as well as at high temperature [1–3] as compared to the neat matrix. It was demonstrated that most mechanical improvements can be imputed to a clear modification of the matrix microstructure induced by the second phases, able to suppress abnormal grain growth and induce a better control of the grain morphology through the well-known *pinning* effect [4,5].

Among the several oxide-based alumina composites already developed [1,2], most studies are currently focused on Al_2O_3/ZrO_2 (zirconia toughened alumina, ZTA) [6–11] and on Al_2O_3/$Y_3Al_5O_{12}$ (YAG) [12–16] particulate composites.

In fact, the dispersion of 5–20 vol.% tetragonal zirconia particles in the alumina matrix can significantly improve the fracture toughness of the neat matrix due to the t/m transformation of zirconia phase under loading. As a result, ZTA is nowadays effectively used in manufacturing of cutting tools, dies or prosthesis components [17]. Alumina–YAG (AY) composites are, indeed, promising for high-temperature applications [13,18–21] thanks to the excellent creep resistance of YAG [22]; in addition, the garnet phase is stable in contact with Al_2O_3 up to 1700 °C [23], which indicates that YAG ought to be a suitable reinforcing phase in alumina matrix.

The synthesis of high purity, nano-crystalline ZTA as well as AY composite powders has been successfully demonstrated in a large number of publications [8,11]. In particular, if wet-chemical routes like sol–gel [24–26] or co-precipitation [27,28] are applied, significant advances in powders features (like purity, chemical homogeneity, particle size and morphology tailoring) can be obtained [28]. In spite of this, the consolidation of nanopowders to full or nearly full density without appreciable grain growth still represents a significant practical challenge; moreover, when composite materials are densified, additional limitations arise from differences in diffusion mechanisms and densification/coarsening temperatures of the phases involved. To overcome

* Corresponding author at: DISMIC, Politecnico di Torino, Corso Duca degli Abruzzi, 24, 10129 Torino, Italy. Tel.: +39 0115644678; fax: +39 011 5644699.
E-mail address: paola.palmero@polito.it (P. Palmero).
[1] Now at: IIT@ POLITO – Centre for Space Human Robotics, C.so Trento 21, 10129 Torino, Italy.

0272-8842/$36.00
doi:10.1016/j.ceramint.2011.06.011

this problem, unconventional sintering techniques have been proposed, such as microwave sintering [29], hot pressing and hot-isostatic-pressing [16,18,19,30] or even new densification technologies, like PECS or SPS [31–33].

However, the real goal in ceramic processing and engineering is to develop manufacturing techniques able to produce large-scale, excellent quality materials at reasonable price.

With this perspective, the manufacturing of Al_2O_3–5 vol.%ZrO_2 (AZ-5) and Al_2O_3–5 vol.%YAG (AY-5) composite powders is here obtained by a simple, reliable method, already described in some previous papers [34–36]. It consists on the surface modification of alumina powders with inorganic precursors of the second phases. Upon heating, different phenomena take place; in fact, in the case of immiscible phases (AZ-5), tetragonal zirconia directly crystallizes on the alumina surface [34] while in the miscible system (AY-5), yttrium diffuses into the alumina bulk and solid-state reaction occurs to produce YAG [35].

With respect to previous works, this paper intends to investigate the role of such miscible and immiscible dopants on the sintering kinetics, during pressure-less processes, and on the microstructural development of the final composites. To achieve such a goal, the densification behaviour of the green ceramic bodies was investigated at several different constant heating rates, in a dilatometer. The results were analysed using an advanced thermokinetic programme module carried out by Opfermann et al. [37], which allowed to predict the sintering behaviour.

The aim of this work is twofold: by one side, to determine the activation energies and the types of reaction for the immiscible (AZ-5) and miscible (AY-5) systems and correlate such parameters to the final microstructures; on the other side, to engineer the sintering cycle by optimizing the density while minimizing the sintering temperature and/or dwell time, thus to obtain a reliable, cost-efficient process.

2. Experimental

A commercial, α-alumina powder (TM-DAR TAIMICRON, supplied by Taimei Chemicals Co., Japan), here referred to as A, was used to develop 95 vol.% alumina–5 vol.% zirconia (AZ-5) and 95 vol.% alumina–5 vol.% YAG (AY-5) nanocomposites. Precursors of the second phases were $ZrCl_4$ (Fluka, >98% purity) and $YCl_3{\cdot}6H_2O$ (Aldrich, 99.99% purity). More details on the powders elaboration method are reported elsewhere [34].

The doped alumina powders were submitted to suitable thermal pre-treatments, with the aim of inducing the second phases crystallization and limiting the residual mass loss during the subsequent sintering. Precisely, AZ-5 was calcined at 600 °C for 1 h (heating and cooling rate of 10 °C/min), thus to induce the crystallization of tetragonal zirconia grains on the alumina surface [34]. The formation of yttrium-aluminates particles requires, indeed, a higher-temperature treatment [34]. Precisely, traces of the monoclinic $Y_4Al_2O_9$ phase were produced on the alumina surface after calcination at 1050 °C for 5 min in AY-5; however, to limit agglomeration during calcination as well as to reduce the second-phase crystallite size, such treatment was carried out through a flash heating [36], by plunging the powder in a tubular furnace kept at the aforementioned temperatures. It should be pointed out that this manufacturing procedure allows the production of highly-pure composite powders; in fact, as demonstrated in a previous paper [34], after calcination at 1500 °C, only tetragonal zirconia is present in AZ-5 samples (even without phase stabilizers) and pure YAG is found in AY-5 materials.

Aqueous suspensions (solid load of 50 wt.%) of A, AZ-5 calcined at 600 °C and of AY-5 flashed heated at 1050 °C, were dispersed by ball-milling, carried out for 48–144 h: as a result, the three powders achieved a similar grain size distribution, with an average agglomerate size of 0.45 μm [34].

Samples A, AZ-5 and AY-5 were uniaxially pressed into bars of 17 mm × 5 mm × 5 mm at 300 MPa and sintered in a dilatometer (Netzsch 402E) up to 1500 (sample A) or to 1550 °C (samples AZ-5 and AY-5) at three different heating rates (precisely at 2, 5 and 10 °C/min), to supply the data required for the modeling of their sintering behaviour by multivariate regression [37]. The determination of the sintering kinetics starts from a model free estimation of activation energies and pre-exponential factors according Ozawa–Flynn–Wall or Friedman [38,39]. Based on these starting data different kinetic models were tested with respect to their prediction quality. A prediction of sintering behaviour of each material was made with the best fitting models to determine optimum sintering parameters (in case of transformation toughened materials, such as AZ-5, this approach leads to the material with the highest hardness but may not lead to the material with the best mechanical properties, such as bending strength and fracture toughness, which require a certain zirconia grain size which is developed by controlled ''oversintering'').

The final density of the composites was determined by Archimedes's method and referred to the respective theoretical density (TD), calculated by the rule of mixture, assuming values of 3.99 g/cm^3 (JCPDS file no. 46-1212), 4.55 g/cm^3 (JCPDS file no. 33-0040) and 6.10 g/cm^3 (JCPDS file no. 79-1763) for α-alumina, YAG and tetragonal ZrO_2, respectively. Precisely, TD of 4.02 and 4.10 g/cm^3 were calculated for AY-5 and AZ-5, respectively.

The microstructures of the fired samples were characterized by SEM (Hitachi S2300) and FESEM (Hitachi S4000); observations were performed on the polished and thermally etched fired samples. Image analysis was carried out on several microstructures, allowing to determine alumina as well as second phase size and distribution.

3. Results and discussion

Table 1 collects the green density of pressed A, AZ-5 and AY-5 samples; we can observe a slightly higher value for A as compared to the composites. The three materials were then sintered at 1500–1550 °C at 2 °C/min, 5 °C/min and 10 °C/min, as detailed in Section 2.

Table 1
Green and fired density of A sintered at 1500 °C and of AZ-5 and AY-5 sintered at 1550 °C at 2 °C/min, 5 °C/min and 10 °C/min (no soaking time).

	Green density, g/cm^3 (%TD)	Fired density (%TD)		
		2 °C/min	5 °C/min	10 °C/min
A	2.27 (57.3)	99.2	99.0	99.0
AZ-5	2.12 (53.0)	98.7	98.5	98.5
AY-5	2.14 (53.2)	99.6	98.2	99.0

The linear shrinkage of alumina green body at constant heating rates is depicted in Fig. 1 in the 800–1500 °C range. The onset sintering temperature was detected at about 1000 °C for all the samples, whereas the maximum densification rate is displayed at higher temperatures while increasing the heating rate. Precisely, it occurs at about 1220, 1250 and 1265 °C at 2 °C/min, 5 °C/min and 10 °C/min, respectively. The same trend was also observed for the composite materials. In spite of these differences, sample A and the composites reached almost full densification, independently from the heating rate, as reported in Table 1.

Fig. 2 shows some representative micrographs of A sintered at 2 °C/min (a), 5 °C/min (b) and 10 °C/min (c). A heterogeneous microstructure can be observed in the first case. In fact, a bimodal grain size distribution is well evident, in which elongated or tabular alumina grains are surrounded by finer, almost equiaxial particles. An average size of 0.71 μm for the equiaxial fraction of grains was determined by image analysis. For the elongated ones, which represent about the 28% of the alumina particles, the aspect ratio (a.r.) was determined, yielding a mean value of 2.6. The sample fired at 10 °C/min presents, on the contrary, a quite monomodal grain size distribution; the microstructure is made by equiaxial alumina grains, while abnormally growth particles were never observed. The grain coarsening observed in the low-rate sintered material was reasonably imputed to the longer exposition time in the high-temperature range. An intermediate situation was finally observed for sample A sintered at 5 °C/min since in this microstructure just few elongated grains were present.

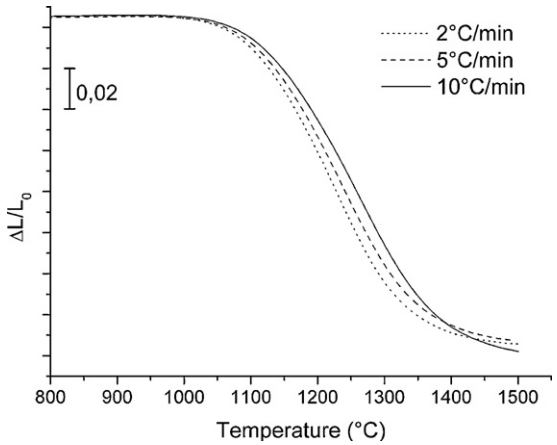

Fig. 1. Linear shrinkage of sample A during sintering up to 1500 °C at 2 °C/min, 5 °C/min and 10 °C/min.

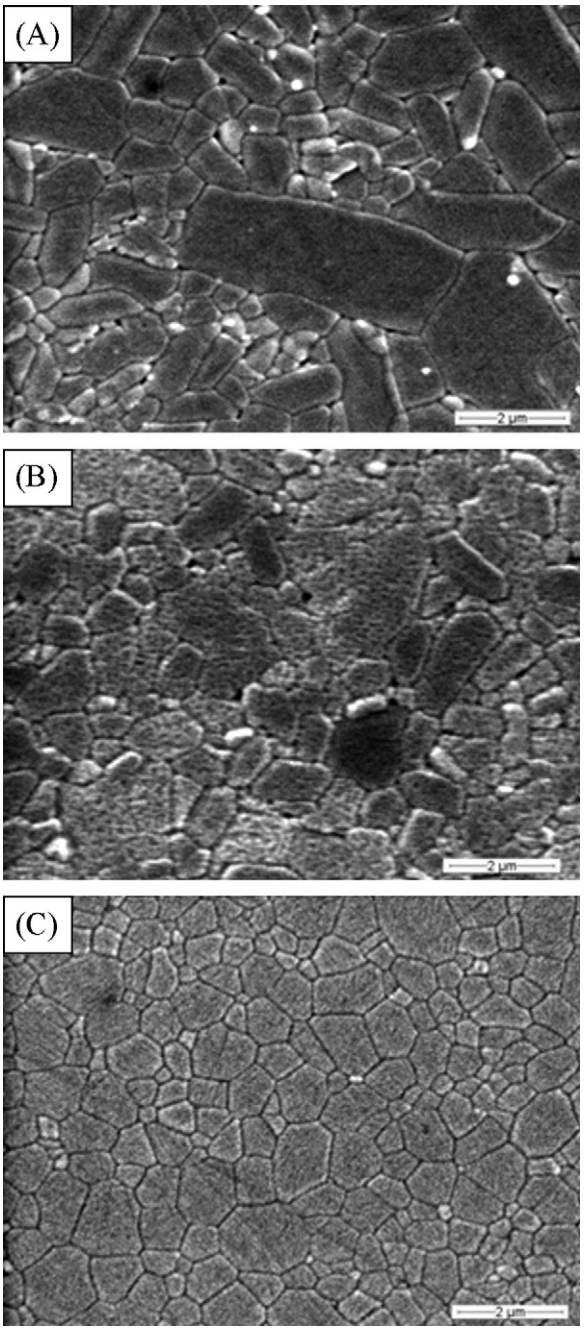

Fig. 2. SEM micrographs of sample A sintered at 1500 °C at 2 °C/min (A), 5 °C/min (B) and 10 °C/min (C).

Similar considerations can be done for AZ-5 nanocomposites, as shown in Fig. 3 for the 2 °C/min (A), 5 °C/min (B) and 10 °C/min (C) fired samples. In this case, a heterogeneous microstructure made by both coarsened and fine alumina grains can be observed in all three materials; however, the lower the heating rate, the higher the amount of coarsened grains. Similar ZTA microstructures were already described in literature [4,40,41], particularly when low zirconia volume fractions were used (up to 5 vol.%) or when the second phase distribution was not sufficiently uniform to hinder the growth of all alumina grains [4]. By observing the three AZ-5 microstructures, a further difference can be pointed out: in fact, in the -low-rate

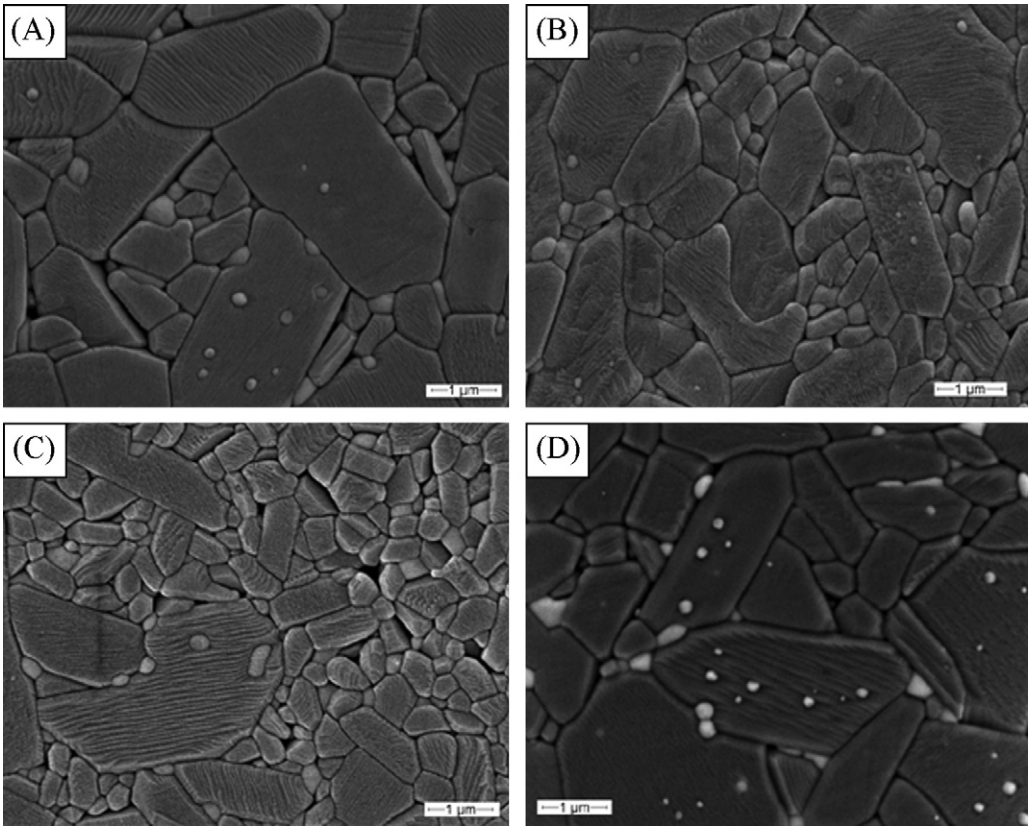

Fig. 3. FESEM micrographs of sample AZ-5 sintered at 1550 °C at 2 °C/min (A), 5 °C/min (B) and 10 °C/min (C); BSE-FESEM image of AZ-5 sintered at 2 °C/min (D).

densified sample, ZrO_2 grains were located at both inter and intra-granular positions, as clearly shown in the BSE image of Fig. 3(D), while a predominant location of zirconia particles in inter-granular positions was observed in the high-rate sintered AZ-5. In both cases, the size of the intra-grains was significantly lower as respect to the inter-ones, as given in Table 2. A similar observation was already reported in literature by Lange and Hirlinger [4], showing a correlation between the alumina growth mechanism and the zirconia distribution and size and explained on the ground of the 2nd phase content in the matrix. According to this work, upon heating the ZrO_2 particles exhibit sufficient self-diffusion to move within the alumina grain boundaries; as a consequence, near the effective dragging force exerted by the second phase, growth of zirconia inclusions (which remain located at inter-granular position) occurs by coalescence. On the contrary, abnormal grain growth appears in the regions with a lower zirconia concentration, where not all the alumina 4-grain junctions are filled: the matrix particles grow into larger ones, while finer zirconia grains are incorporated.

A different microstructural development was finally presented by the AY-5 samples (Fig. 4), since in these materials elongated or even abnormally growth alumina grains were never observed, independently from the heating rate. However, for both alumina and YAG phases, slightly higher average grain size was found by lowering the heating rate. In all samples YAG

Table 2
Average grain size and standard deviation of equiaxial Al_2O_3, ZrO_2 and YAG particles and aspect ratio (a.r.) of the elongated Al_2O_3 grains in A and AZ-5 and AY-5 nanocomposites.

Sample	Equiaxial Al_2O_3 grains (μm)	Elongated Al_2O_3 grains (a.r.)	Inter-ZrO_2 grains (μm)	Intra-ZrO_2 grains (μm)	Inter-YAG grains (μm)	Intra-YAG grains (μm)
A—10 °C/min	0.65 ± 0.33	–	–	–	–	–
A—5 °C/min	0.70 ± 0.30	Few	–	–	–	–
A—2 °C/min	0.71 ± 0.20	2.61 ± 0.60	–	–	–	–
AZ—5–10 °C/min	0.40 ± 0.33	2.46 ± 0.47	0.34 ± 0.03	0.20 ± 0.07	–	–
AZ—5–5 °C/min	0.55 ± 0.21	2.57 ± 0.51	0.35 ± 0.04	0.20 ± 0.03	–	–
AZ—5–2 °C/min	0.65 ± 0.11	2.35 ± 0.39	0.46 ± 0.05	0.14 ± 0.02	–	–
AY—5–10 °C/min	0.76 ± 0.28	–	–	–	0.30 ± 0.01	0.18 ± 0.06
AY—5–5 °C/min	0.93 ± 0.32	–	–	–	0.31 ± 0.03	0.21 ± 0.07
AY—5–2 °C/min	0.97 ± 0.48	–	–	–	0.35 ± 0.01	0.20 ± 0.07

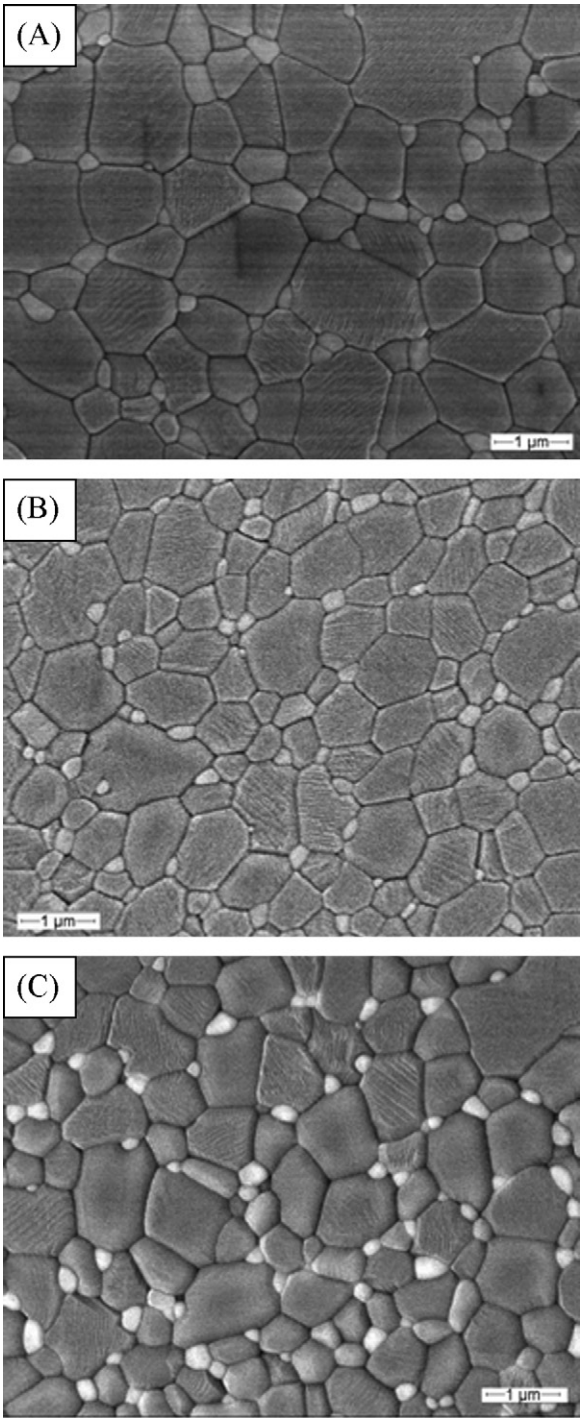

Fig. 4. FESEM micrographs of sample AY-5 sintered at 1550 °C at 2 °C/min (A), 5 °C/min (B) and 10 °C/min (C).

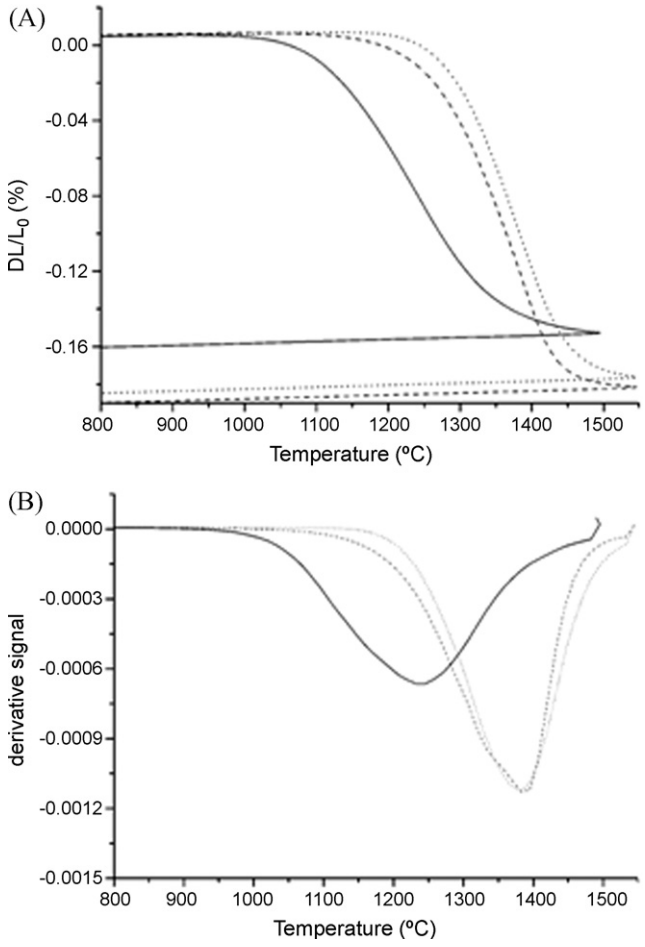

Fig. 5. Sintering (A) and derivative (B) curves in the 800–1550 °C range at the heating rate of 5 °C/min for sample A (solid line) and for AZ-5 (dashed line) and AY-5 (dotted line) composites.

was predominantly located in inter-granular positions; when observed, the intra-grains were again characterized by a smaller size as compared to the inter ones. A possible explanation for the different microstructures observed in samples AZ-5 and AY-5 is presented in the followings.Dilatometry data of all materials were imported to Netzsch Thermokinetics software and best fitting models were determined. Different sintering behaviour of the three materials becomes clear upon comparing their dilatometry curves in one diagram: as an example, Fig. 5 reports the sintering (A) and the derivative (B) curves of the three materials collected at 5 °C/min. While the sintering of A starts at 1000 °C, sintering of both composites is delayed to 1100 °C (AZ-5) and 1150 °C (AY-5), as already stated by literature [34–36]. In addition, second phases also rise the temperature of maximum sintering rate in comparison with pure alumina as shown by the derivative curves in Fig. 5(B). We can observe, in fact, that A has a very flat sintering curve with a maximum densification rate at 1250 °C, while the very steep curves of AY-5 and AZ-5 look very similar with maximum densification rates at 1350 °C (AZ-5) and 1375 °C (AY-5).

The steeper slope of the composites hints at higher activation energies; this assumption is confirmed by the results of model-free estimations of activation energy (Fig. 6). In fact the activation energy of A declines from 1500 to 800 kJ/mol with proceeding densification. AY-5 and AZ-5 show an almost identical scheme with constant activation energy of ∼1000 kJ/mol between 0% and 80% densification and a final rise to 1700 kJ/mol in the final densification stage. This rise hints at a change in mechanism and at a sluggish densification behaviour in the final stage requiring much higher sintering temperatures than A. (The higher standard deviation of activation energies in A can be explained by the much lower quality of raw data; in the

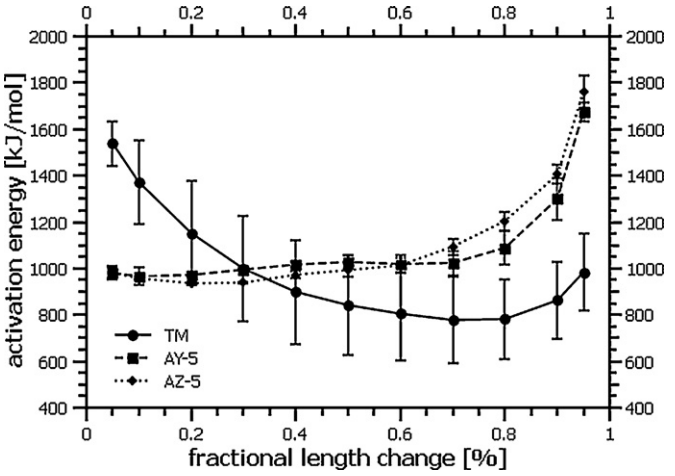

Fig. 6. Activation energy vs. fractional length change for A, AZ-5 and AY-5 samples.

final stage a crossover of two curves 5 °C/min and 10 °C/min was observed.)

For alumina two models were tested, a single stage Avrami–Erofeev nucleation and growth model (An) and a two stage model with a subsequent power law step (AnFn).

The length change with time in an Avrami–Erofeev type kinetics can be described by a formula of the type:

$$\frac{dl}{dt} = -k_0 e^{-(E_A/RT)} n l(-\ln(l))^{(n-1)/n} \quad (1)$$

with l = length, n = nucleation dimension and k_0 = pre-exponential factor, E_A = activation energy. Evidently a reduction in n leads to an acceleration of length change.

In a power-law kinetics, length change velocity can be described by a formula of the type:

$$\frac{dl}{dt} = -k_0 e^{-(E_A/RT)} l^n \quad (2)$$

A high formal reaction order leads to a low reaction rate at high fractional length change.

The results are summarized in Table 3. The two stage model leads to higher prediction quality and an activation energy of about 1100 kJ/mol for the first step and an activation energy of about 800 kJ/mol for the second step. Standard deviations show a relatively high scattering of modeling data, a fact which was already revealed in the model-free estimation. Introduction of a third reaction step (not shown) did not lead to a further refinement in model quality and was thus not further considered.

The AY-5 composite (Table 4) also reaches the best fit quality with the two stage Avrami–Erofeev and subsequent power law reaction (AnFn). The rise in activation energy with increasing densification (see Fig. 6) is well represented as well as the fraction of reaction 1 (70% fits well with model-free estimation data). Compared to the model of sample A the fit quality is significantly improved.

As mentioned, the AZ-5 composite behaves very similar to the AY-5 material. Best fit quality was obtained with the two stage Avrami–Erofeev and subsequent power law reaction (AnFn) (see Table 5). Reaction 1 covers 80% of densification, reaction 2 with higher activation energy covers the final densification reaction. Prediction quality of the AZ-5 model was the best of all three models.

As an example, Fig. 7 compares the sintering curves of AY-5 at the three heating rates with fits given by Avrami–Erofeev

Table 3
Kinetic parameters for 1-stage and 2-stage models calculated for A.

Model	log A_1 (s^{-1})[a]	Ea_1 (kJ/mol)[b]	Nucl. f. 1[c]	log A_2 (s^{-1})[a]	Ea_2 (kJ/mol)[b]	Order 2[d]	Foll-react. 1[e]	Corr. coeff.	Least squares	Durbin–Watson
An	29.41 ± 17.87	941 ± 520	0.229 ± 0.112	–	–	–	–	0.9988	81	5.72
AnFn	36.46 ± 6.92	1095 ± 196	0.273 ± 0.055	23.66 ± 7.08	789 ± 204	3.11 ± 0.68	0.593 ± 0.153	0.9998	12	4.26

[a] log A_n (s^{-1}): logarithm of the pre-exponential of reaction step n.
[b] Ea_n: activation energy of reaction step n.
[c] Nucl. f. 1: nucleation factor of reaction step 1.
[d] Order 2: order of reaction for reaction step 2.
[e] Foll-react. 1: portion of total shrinkage of consecutive reaction 1.

Table 4
Kinetic parameters for 1-stage and 2-stage models calculated for AY-5.

Model	log A_1 (s^{-1})[a]	Ea_1 (kJ/mol)[b]	Nucl. f. 1[c]	log A_2 (s^{-1})[a]	Ea_2 (kJ/mol)[b]	Order 2[d]	Foll-react. 1[e]	Corr. coeff.	Least squares	Durbin–Watson
An	29.75 ± 5.85	1026 ± 183	0.373 ± 0.057	–	–	–	–	0.9996	37.4	3.88
AnFn	29.15 ± 0.84	986 ± 27	0.477 ± 0.0055	32.55 ± 1.85	1136 ± 60	2.48 ± 0.12	0.689 ± 0.052	0.9999	1.98	2.04

[a] log A_n (s^{-1}): logarithm of the pre-exponential of reaction step n.
[b] Ea_n: activation energy of reaction step n.
[c] Nucl. f. 1: nucleation factor of reaction step 1.
[d] Order 2: order of reaction for reaction step 2.
[e] Foll-react. 1: portion of total shrinkage of consecutive reaction 1.

Table 5
Kinetic parameters for 1-stage and 2-stage models calculated for AZ-5.

Model	log A_1 (s^{-1})[a]	Ea_1 (kJ/mol)[b]	Nucl. f. 1[c]	log A_2 (s^{-1})[a]	Ea_2 (kJ/mol)[b]	Order 2[d]	Foll-react. 1[e]	Corr. coeff.	Least squares	Durbin–Watson
An	30.0 ± 0.88	1023 ± 183	0.335 ± 0.057	–	–	–	–	0.9998	10.3	2.28
AnFn	28.52 ± 0.8	963 ± 27	0.377 ± 0.0117	35.81 ± 2.48	1236 ± 69	2.53 ± 0.19	0.799 ± 0.036	0.9999	3.4	1.833

[a] log A_n (s^{-1}): logarithm of the pre-exponential of reaction step n.
[b] Ea_n: activation energy of reaction step n.
[c] Nucl. f. 1: nucleation factor of reaction step 1.
[d] Order 2: order of reaction for reaction step 2.
[e] Foll-react. 1: portion of total shrinkage of consecutive reaction 1.

(An) and subsequent power law reaction (AnFn), showing a very good match between experimental and modeling data.

The main difference which leads to the delay in sintering onset of AY-5 compared to AZ-5 is the higher nucleation factor of the first reaction while pre-exponential factors and activation energies are almost identical.

Please note that the models are purely macrokinetic approaches (black box) which do not directly allow for describing what happens at microstructural scale. The result thus has to be ''translated'' to correlate the model and its parameters to processes taking place during sintering. Activation energies and pre-exponential factors can be easily understood as parameters with real kinetic significance.

Nucleation factors and reaction orders are more difficult to understand as neither reactions nor nucleation actually take place in the ceramics. It is obvious that all phases are present from the beginning and grains may coalesce but no new nuclei are formed. A nucleation dimension of <1 has no physical meaning. Nucleation dimensions and reaction orders are related to the kinetics of different diffusion phenomena taking place in the ceramics during sintering. In a very simplified manner, it may be stated that ''nucleation'' in the models used for sintering is related to diffusion processes leading to no or little volume change. E.g. surface diffusion and volume diffusion starting from the surface do not lead to densification but they reduce the free surface area and increase the area of the grain boundary which in the next stage results in densification processes starting from the grain boundaries.

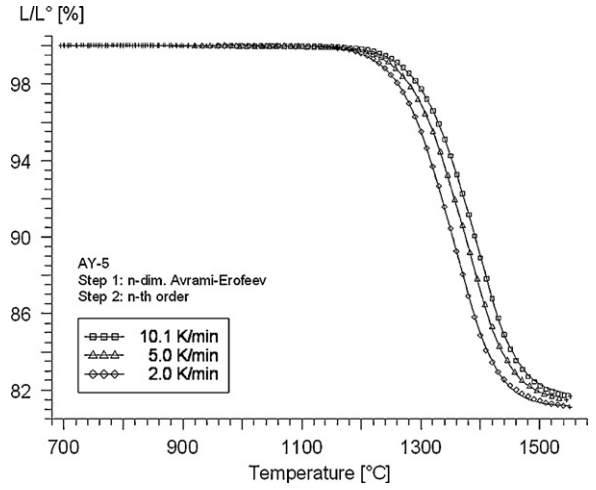

Fig. 7. Sintering curves of AY-5 and relative fits given by Avrami–Erofeev (An) and subsequent power law reaction (AnFn) at 2 °C/min, 5 °C/min and 10 °C/min.

As only volume diffusion starting from grain boundaries and grain boundary diffusion lead to densification it may be stated that the addition of a second phase no matter if miscible or immiscible changes the kinetics of these two processes. One may suspect that yttria which forms a very diffusion resistant grain boundary film may be very efficient to retard these processes, the result can be seen in the late onset of densification described by higher activation energy and high nucleation factor. In fact, a previous paper [35] demonstrated that such yttrium-rich film homogeneously coated the alumina particles, up to high temperature (about 1300 °C). Above this value, and while proceeding with densification, yttrium started to diffuse and formed yttrium-richer areas at alumina grain boundaries or at triple points, finally giving rise to precipitation of yttrium-aluminates. Such hypothesis well matches the AY-5 microstructures presented in Fig. 4, in which only intergranular YAG particles were observed, homogeneously distributed into a fine-grained alumina matrix.

In alumina, diffusion processes along the grain boundaries are not inhibited.

In the case of AZ-5 the processes are different. It is assumed that the constituent phases are (almost) immiscible. Thus, a retarding effect of a diffusion resistant film on the grain surface can be ruled out. The numerous zirconia grains (already crystallized at the temperatures involved with the sintering process) on the surface do however prevent the converging of the alumina grains. It requires some activation to grow the nanoparticles, thus reduce their number, and create larger sites where alumina grains do actually touch and develop grain boundary areas where diffusion can proceed. The bimodal alumina grain size distribution in this material (see Fig. 3) can be due to ineffective pinning of the low zirconia amount at alumina grain boundaries, as previously discussed. As an alternative explanation, we can hypothesise very strong grain boundaries between alumina and zirconia, so that alumina will rather grow around the zirconia grains than ''push'' them aside to triple points. In the final stage the second phase trapped in triple points (as in AY-5) of the alumina grains would disturb the formation of regular cube-octahedrons and act as a grain refinement. In fact the alumina–zirconia grain boundaries seem to be so strong that zirconia grains are incorporated and alumina exhibits abnormal grain growth.

Based on these models, predictions of sintering behaviour were simulated. The graphs for the three materials are shown in Fig. 8, assuming an infinitely fast heating to final temperature.

For sample A (a), assuming a dwell time of 3 h, a final sintering temperature of 1375–1425 °C is required to achieve full densification. AY-5 (b), despite the small grain size of the starting powder, requires sintering temperatures of >1450 °C to reach full density at 3 h dwell. AZ-5 (c) requires 1400–1425 °C at 3 h dwell for full densification. Following the above predictions samples A and AZ-5 were densified at 1425 °C/3 h, while AY-5 was sintered at 1475 °C/3 h (heating rate of 5 °C/min), reaching full densification (99.9%TD for A, 99.8%TD for AZ-5 and 99.7%TD for AY-5). Fig. 9 collects the related fired microstructures.

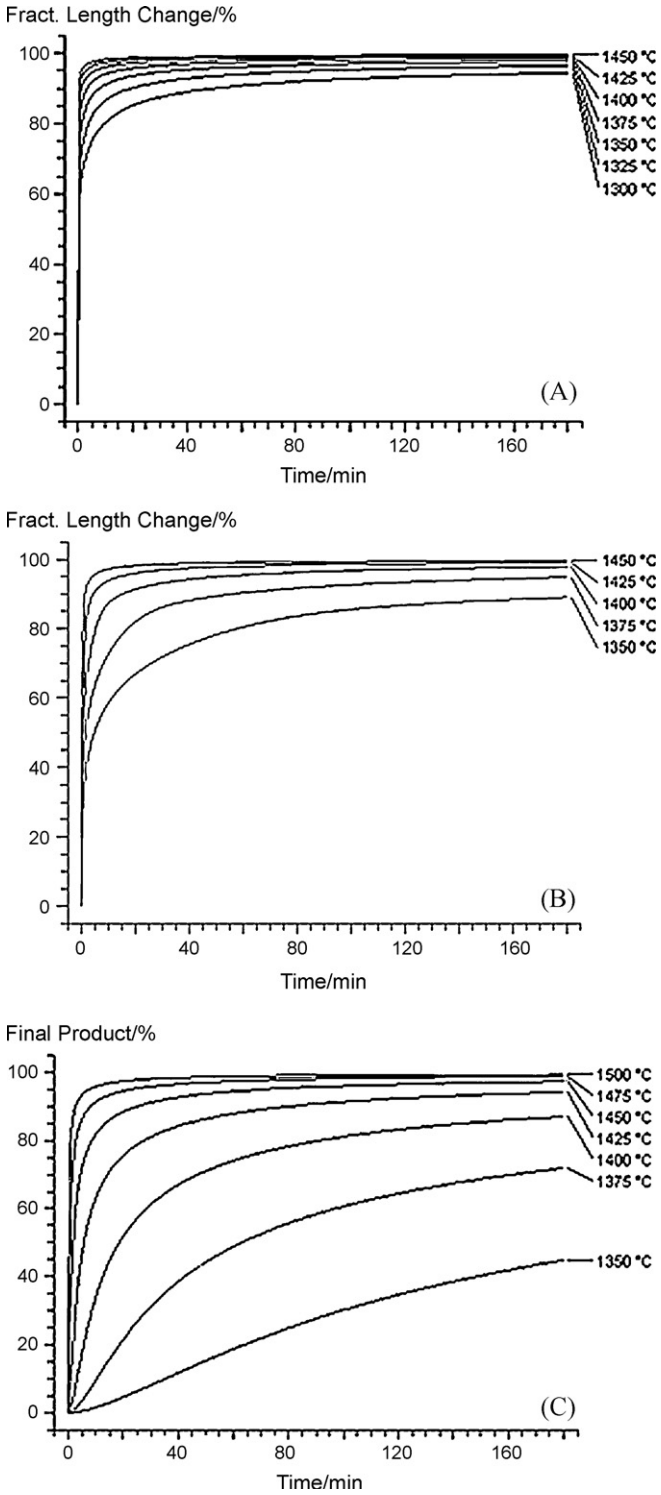

Fig. 8. Prediction of sintering behaviour in isothermal conditions for A (A), AZ-5 (B) and AY-5 (C) samples.

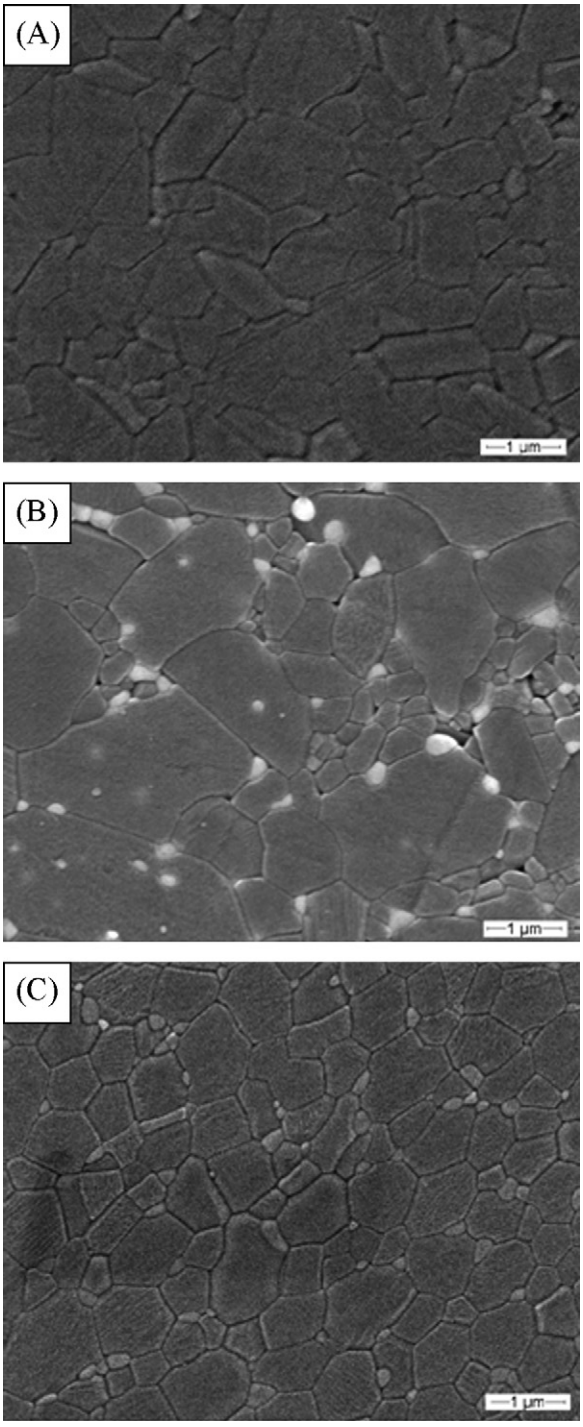

Fig. 9. FESEM images of samples A (A) and AZ-5 (B) sintered at 1425 °C/3 h and of AY-5 (C) sintered at 1475 °C/3 h.

In the case of sample A (Fig. 9A), a highly dense microstructure was yielded, in which some tabular grains were still observed. An average alumina grain size of 0.88 μm (±0.35) was determined.

Fig. 9(B) shows the fired microstructure of AZ-5. We still observe a certain bimodal distribution of alumina grain size, with both inter and intra-granular ZrO_2 grains. Image analysis supplied an average size of 0.29 (±0.09) and of 0.13 (±0.05) for inter and intra-particles, respectively, confirming a statistical smaller grain size for these last ones.

A homogenous microstructure was indeed observed in AY-5 (Fig. 9C): inter-granular YAG grains, having an average size of 0.24 μm (±0.06) were homogeneous distributed into the alumina matrix, whose average size was 0.72 μm (±0.26). It is interesting to note that alumina matrix is even finer in AY-5 sintered at 1475 °C than in the monolithic material densified at 1425 °C, thus denoting an important pinning effect of YAG in the former case.

In spite of a mechanical characterization is not the aim of this paper, we can reasonably suppose that the AY-5 developed microstructure and its very high density could make this material a potential candidate for high-temperature applications [20].

In contrast, the ultra-fine size of tetragonal zirconia in AZ-5 may not assure reasonable toughness, due to inhibited transformation into monoclinic phase [40]. So, in order to develop microstructures able to assure high mechanical performances, AZ-5 maximum sintering temperature was even increased in the range 1450–1475 °C. In Fig. 10, the microstructure of the sample sintered at 1475 °C for 3 h is reported: once again, coarsened alumina particles were observed, while average sizes for inter and intra-granular ZrO_2 of 0.4 μm (±0.17) and 0.16 μm (±0.07) were respectively determined. If a comparison (at the same heating rate of 5 °C/min) with values given in Table 2 is made, a slightly higher average size for the inter-granular ZrO_2 fraction was here found, thus evidencing that a significant grain growth of zirconia grains occurred during the 3-h dwelling at 1475 °C. Additionally, we should mention that, in spite of the heterogeneous microstructure presented by the alumina matrix in AZ-5 composites, the zirconia distribution was quite homogeneous, as shown in the lower-magnification image of Fig. 10(B).

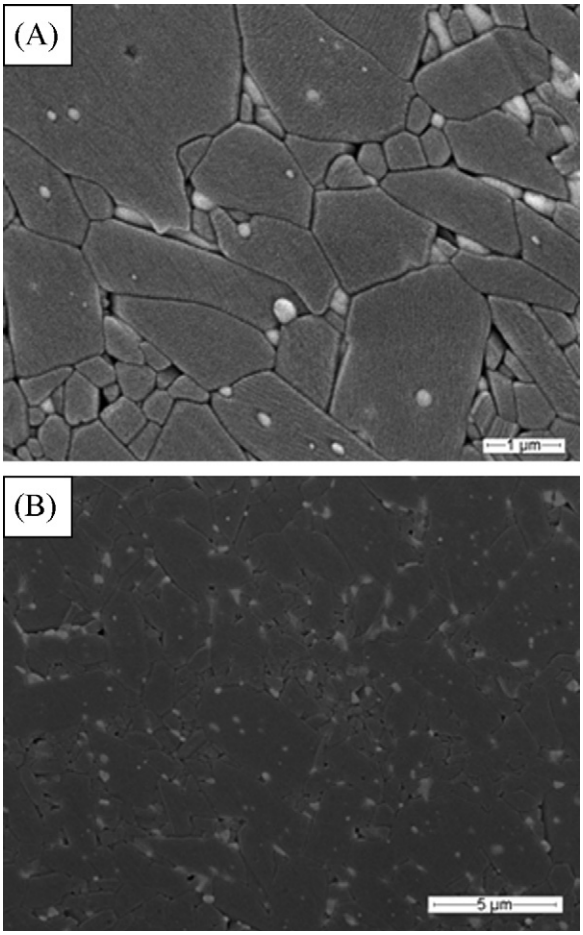

Fig. 10. High (A) and low (B) magnifications FESEM images of AZ-5 sintered at 1475 °C/3 h.

Finally, as an overall comment on this work, it was surprising and instructive to see that two materials with – *a priori* – totally different characteristics, AZ-5 and AY-5 with very different final microstructures and chemical composition develop an almost identical macrokinetic behaviour in sintering. Thus the type of sinter modeling used can be employed as a very useful engineering tool to optimize the sintering cycles of new material compositions. However, conclusions referring to microstructural changes (''microkinetics'') have to made with extreme care and require verification by observation of microstructural changes during the sintering process in order not to come to wrong interpretations.

4. Conclusions

The sintering behaviour and the microstructural development of two composite materials, precisely, Al_2O_3–5 vol.%ZrO_2 (AZ-5) and Al_2O_3–5 vol.%YAG (AY-5), are here investigated and compared to that of a pure alumina sample (A).

Pressed bars of the above powders were pressureless-sintered in a dilatometer at 2 °C/min, 5 °C/min and 10 °C/min up to 1500 °C (sample A) and 1550 °C (samples AZ-5 and AY-5), yielding fully dense bodies.

A critical role of the heating rate on the fired microstructures was evidenced since the lower the heating rate the higher the average grain size of the reinforcing phases.

In addition, A produced a homogeneous microstructure if heated at 10 °C/min, while coarsened, elongated grains were progressively observed by decreasing the heating rate. A bimodal alumina grain size distribution was even observed in AZ-5 samples, independently from the heating rate, even if with a higher extent in the 2 °C/min heated sample. Finally, in AY-5, homogeneous microstructures were always observed.

The experimental sintering curves of the three materials were very well fit by using an Avrami–Erofeev nucleation and growth model (An) and a subsequent power law reaction (AnFn), here employed to evaluate activation energy, nucleation factors as well as reaction orders and types for the three materials. In

addition, densification mechanisms for the composites have been hypothesized and correlated with the developed fired microstructures.

Finally, the modeling approach was also successfully employed to predict the best sintering conditions for sample A (1375–1425 °C/3 h), AY-5 (1450–1475 °C/3 h) and AZ-5 (1425 °C/3 h), resulting in fully dense materials with more controlled microstructural features.

References

[1] A.G. Evans, Perspective on the development of high-toughness ceramics, J. Am. Ceram. Soc. 73 (1990) 187–206.

[2] M. Sternitzke, Review: structural ceramic nanocomposites, J. Eur. Ceram. Soc. 17 (1997) 1061–1082.

[3] T. Ohji, Strengthening and toughening mechanism of ceramic nanocomposites, J. Am. Ceram. Soc. 81 (1998) 1453–1460.

[4] F.F. Lange, M.M. Hirlinger, Hindrance of grain growth in Al_2O_3 by ZrO_2 inclusions, J. Am. Ceram. Soc. 67 (1984) 164–168.

[5] C.J. Lin, W.C.I. Wie, Grain boundary pinning of polycrystalline Al_2O_3 by Mo inclusions, Mater. Chem. Phys. 111 (2008) 82–86.

[6] J. Chevalier, S. Grandjean, M. Kuntz, G. Pezzotti, On the kinetics and impact of tetragonal to monoclinic transformation in an alumina/zirconia composite for arthroplasty applications, Biomaterials 30 (2009) 5279–5282.

[7] J.M. Calderon-Moreno, M. Schehl, M. Popa, Superplastic behavior of zirconia-reinforced alumina nanocomposites from powder alcoxide mixtures, Acta Mater. 50 (2002) 3973–3983.

[8] R.K. Sadangi, V. Shukla, B.H. Kear, Processing and properties of $ZrO_2(3Y_2O_3)$–Al_2O_3 nanocomposites, Int. J. Refract. Met. Hard. Mater. 23 (2005) 363–368.

[9] F.A.T. Guimaraes, K.L. Silva, V. Trombini, J.J. Pierri, J.A. Rodrigues, R. Tomasi, E.M.J.A. Pallone, Correlation between microstructure and mechanical properties of Al_2O_3/ZrO_2 nanocomposites, Ceram. Int. 35 (2009) 741–745.

[10] W.H. Tuan, R.Z. Chen, T.C. Wang, C.H. Cheng, P.S. Kuo, Mechanical properties of Al_2O_3/ZrO_2 composites, J. Eur. Ceram. Soc. 22 (2002) 22827–22833.

[11] D. Gutknecht, J. Chevalier, V. Garnier, G. Fantozzi, Key role of processing to avoid low temperature aging in alumina zirconia composites for orthopedic applications, J. Eur. Ceram. Soc. 27 (2007) 1547–1552.

[12] J.D. French, M.P. Harmer, H.M. Chan, G.A. Miller, Coarsening-resistant dual-phase interpenetrating microstructures, J. Am. Ceram. Soc. 73 (1990) 2508–2510.

[13] R. Torrecillas, M. Schehl, L.A. Diaz, J.L. Menendez, J.S. Moya, Creep behaviour of alumina/YAG nanocomposites obtained by a colloidal processing route, J. Eur. Ceram. Soc. 27 (2007) 143–150.

[14] B.K. Jang, M. Enoki, T. Kishi, H.K. Oh, Effect of second phase on mechanical properties and toughening of Al_2O_3 based ceramic composites, Compos. Eng. 5 (1995) 1275–1286.

[15] W.Q. Li, L. Gao, Processing, microstructure and mechanical properties of 25 vol.% YAG–Al_2O_3 nanocomposites, Nanostruct. Mater. 11 (1999) 1073–1080.

[16] H. Wang, L. Gao, Z. Shen, M. Nygren, Mechanical properties and microstructures of Al_2O_3–5 vol.% YAG composites, J. Eur. Ceram. Soc. 21 (2001) 779–783.

[17] T. Sornakumar, M.V. Gopalakrishnan, R. Krishnamurthy, C.V. Gokularathnam, Development of alumina and Ce-TTZ ceramic–ceramic composite (ZTA) cutting tool, Int. J. Refract. Met. Hard. Mater. 13 (1995) 375–378.

[18] J.D. French, H.M. Chan, M.P. Harmer, G.A. Miller, High-temperature fracture toughness of duplex microstructures, J. Am. Ceram. Soc. 79 (1996) 58–64.

[19] J.D. French, J. Zhao, M.P. Harmer, H.M. Chan, G.A. Miller, Creep of duplex microstructures, J. Am. Ceram. Soc. 77 (1994) 2865–2875.

[20] H. Duong, J. Wolfenstine, Creep behaviour of fine-grained two-phase Al_2O_3–$Y_3Al_5O_{12}$ materials, Mater. Sci. Eng. A 172 (1993) 173–179.

[21] L.N. Satapathy, A.H. Chokshi, Microstructural development and creep deformation in an alumina–5% yttrium aluminium garnet composite, J. Am. Ceram. Soc. 88 (2005) 2848–2854.

[22] A.T. Parthasarathy, T. Mah, K. Keller, Creep mechanism of polycrystalline yttrium aluminium garnet, J. Am. Ceram. Soc. 75 (1992) 1756–1759.

[23] T. Mah, T.A. Parthasarathy, L.E. Matson, Processing and mechanical properties of $Al_2O_3/Y_3Al_5O_{12}$ (YAG) eutectic composite, Ceram. Eng. Sci. Proc. 11 (1990) 1617–1627.

[24] M. Balasubramanian, T. Sornakumar, S.K. Malhorta, C.V. Gokularathnam, R. Krishnamurthy, Grinding of sol–gel derived alumina–zirconia composites, Int. J. Refract. Met. Hard. Mater. 13 (1995) 359–363.

[25] B.T. Lee, J.K. Han, F. Saito, Microstructure of sol–gel synthesized Al_2O_3–ZrO_2 (Y_2O_3) nano-composites, Mater. Sci. Eng. 59 (2005) 355–360.

[26] S.A. Hassanzadeh-Tabrizi, E. Taheri-Nassaj, H. Sarpoolaky, Synthesis of an alumina–YAG nanopowder via sol–gel method, J. Alloys Compd. 456 (2008) 282–285.

[27] Y. Matsumoto, K. Hirota, O. Yamaguchi, S. Inamura, H. Miyamoto, N. Shiokawa, K. Tsuji, Mechanical properties of isostatically pressed zirconia toughened alumina ceramics prepared from coprecipitated powders, J. Am. Ceram. Soc. 76 (1993) 2677–2680.

[28] W.Q. Li, L. Gao, Co-precipitation processed needle-like YAG dispersed in alumina powder, Mater. Lett. 48 (2001) 157–161.

[29] R.R. Menezes, R.H.A.G. Kiminami, Microwave sintering of alumina–zirconia nanocomposites, J. Mater. Process. Technol. 203 (2008) 513–517.

[30] A.H. De Aza, J. Chevalier, G. Fantozzi, M. Schehl, R. Torrecillas, Crack growth resistance of alumina, zirconia and zirconia toughened alumina ceramics for joint prostheses, Biomaterials 23 (2002) 937–945.

[31] L. Gao, Z. Shen, M. Miyamoto, Superfast densification of oxide/oxide ceramic composites, J. Am. Ceram. Soc. 82 (1999) 1061–1063.

[32] D.D. Jayaseelan, N. Kondo, D. Amutha Rani, S. Ueno, T. Ohji, S. Kanzaki, Pulse electric current sintering of Al_2O_3/3 vol% ZrO_2 with constrained grains and high strength, J. Am. Ceram. Soc. 85 (2002) 2870–2872.

[33] V. Trombini, E.M.J.A. Pallone, U. Anselmi-Tamburini, Z.A. Munir, R. Tomasi, Characterization of alumina matrix nanocomposite with ZrO_2 inclusions densified by spark plasma sintering, Mater. Sci. Eng. A 501 (2009) 26–29.

[34] P. Palmero, V. Naglieri, J. Chevalier, G. Fantozzi, L. Montanaro, Alumina-based nanocomposites obtained by doping with inorganic salt solutions: application to immiscible and reactive systems, J. Eur. Ceram. Soc. 29 (2009) 59–66.

[35] P. Palmero, C. Esnouf, Phase and microstructural evolution of yttrium-doped nanocrystalline alumina: a contribution of advanced microscopy techniques, J. Eur. Ceram. Soc. 31 (2011) 507–516.

[36] P. Palmero, V. Naglieri, G. Spina, M. Lombardi, Microstructural design and elaboration of multiphase ultra-fine ceramics, Ceram. Int. 37 (2011) 139–144.

[37] J. Opfermann, J. Blumm, W.D. Emmerich, Simulation of the sintering behaviour of a ceramic green body using advanced thermokinetic analysis, Thermochim. Acta 318 (1998) 213–220.

[38] T. Ozawa, A new method of analyzing thermogravimetric data, Bull. Chem. Soc. Jpn. 38 (1965) 1881–1886.

[39] H.L. Friedman, Kinetics of degradation of char forming plastics from thermogravimetry, application to phenolic plastic, J. Polym. Sci. Part C 6 (1964) 183–195.

[40] D.J. Green, Critical microstructures for microcracking in Al_2O_3–ZrO_2 composites, J. Am. Ceram. Soc. 65 (1982) 610–614.

[41] J. Chevalier, S. Deville, G. Fantozzi, J.F. Bartolomè, C. Pecharroman, J.S. Moya, L.A. Diaz, R. Torrecillas, Nanostructured ceramic oxides with a slow crack growth resistance close to covalent materials, Nano Lett. 5 (2005) 1297–1301.